JCTC Journal of Chemical Theory and Computation

Article

pubs.acs.org/JCTC

Accurate Excited State Geometries within Reduced Subspace TDDFT/TDA

David Robinson*

School of Chemistry, University Of Nottingham, University Park, Nottingham NG7 2RD, United Kingdom

Supporting Information

ABSTRACT: A method for the calculation of TDDFT/TDA excited state geometries within a reduced subspace of Kohn−Sham orbitals has been implemented and tested. Accurate geometries are found for all of the fluorophore-like molecules tested, with at most all valence occupied orbitals and half of the virtual orbitals included but for some molecules even fewer orbitals. Efficiency gains of between 15 and 30% are found for essentially the same level of accuracy as a standard TDDFT/TDA excited state geometry optimization calculation.

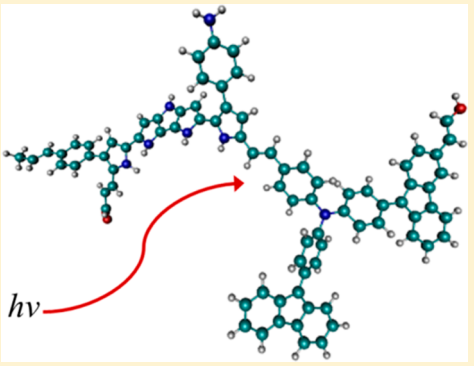

1. INTRODUCTION

Excited-state electronic structure geometry calculations are a vital method for understanding excited-state properties within a relaxed geometrical structure. In particular, obtaining such a geometry is a key point in the calculation of fluorescence emission spectra and conical intersections, to name but two. Traditionally, methods such as complete active space self-consistent field (CASSCF)[1] and various flavours of multi-reference perturbation theory, for example, CASPT2,[2,3] MRMP2,[4,5] NEVPT2,[6−8] have been used to obtain such geometries, with a great deal of success and accuracy. Unfortunately, even with advances in algorithms[9] and various truncation approximations,[10−14] such methods are limited to relatively small molecules. Equation-of-motion coupled-cluster methods (EOM-CC) provide a highly accurate single reference approach, but these approaches are also limited to relatively small molecules.[15−22] In the past decade or so, time-dependent density functional theory (TDDFT) has proven a cheap and fairly reliable method for calculating excited-state energies, structures, and properties, especially since the advent of analytical gradients.[23−29] While there are situations in which conventional functionals within the TDDFT framework are known to fail,[30] there are solutions to this allowing calculation of accurate energies and geometries for much larger molecules than is possible with the more accurate multireference strategies. TDDFT has advantages over its cheaper alternative, maximum-overlap method (MOM);[31] MOM is known to incorrectly describe singlet excited states when they resemble an open-shell singlet, while TDDFT can correctly describe such states.

Within the field of TDDFT, there have been a few approximations that have reduced the computational cost of the calculation of the vertical excitation energies, with negligible effect upon quantitative accuracy. The Tam−Dancoff approximation[32] has reduced the dimension of the TDDFT equations by a factor of 2 while generally maintaining a similar level of accuracy, although for some molecular species there are significant discrepancies.[33] A second method, in which a reduced subspace of orbitals are included within the TDDFT calculation,[34] has proven very effective approximations for reducing computational effort. Very little loss of accuracy of the excitation energies is observed, while a small degradation in the quantitative accuracy of the oscillator strength has been observed. This method has been successfully applied to molecules in solvent,[35,36] on surfaces,[37−39] chromophores within protein environments,[40−43] within membrane environments[44] and also to the calculation of core excited states,[45−47] necessary for understanding near-edge X-ray absorption fine spectra (NEXAFS).

In the current study, we investigate the use of the reduced subset of single-excitations, within the framework of an extremely limited set of occupied and virtual orbitals, upon the accuracy of calculated excited-state geometries in comparison to conventional (all-orbital) TDDFT geometries (within the Tamm−Dancoff approximation), and also to determine the computational efficiency of such an approach.

2. COMPUTATIONAL DETAILS

The first singlet excited-state geometries of a range of small to medium sized molecules were optimized using TDDFT/TDA with the B3LYP,[48] LRC-ωPBE,[49] and ωB97X-D[50] functionals and 6-31G(d)[51] and 6-311G(d)[52] basis sets. These functionals were chosen as representative examples of those commonly

Received: July 31, 2014

dx.doi.org/10.1021/ct500687j | J. Chem. Theory Comput. XXXX, XXX, XXX−XXX

Table 1. Emission Energy Differences Calculated between Conventional TDDFT/TDA and the Reduced Subspace TDDFT/TDA[a] at the First Singlet Excited-State Geometry Calculated with the Respective Method[b]

		functional		
molecule	basis set	B3LYP	LRC-ωPBE	ωB97X-D
formaldehyde	6-31G(d)	0.023 (0.8%)	0.027 (0.9%)	0.015 (0.5%)
	6-311G(d)	0.021 (0.7%)	0.021 (0.7%)	0.008 (0.3%)
benzene	6-31G(d)	0.042 (0.8%)	0.045 (0.8%)	0.044 (0.8%)
	6-311G(d)	0.044 (0.8%)	0.049 (0.9%)	0.048 (0.9%)
naphthalene	6-31G(d)	0.036 (0.8%)	0.146 (3.2%)	0.105 (2.3%)
	6-311G(d)	0.037 (0.9%)	0.145 (3.2%)	0.106 (2.3%)
indole	6-31G(d)	[d]	0.317 (6.3%)	0.150 (3.0%)
	6-311G(d)	[d]	0.319 (6.4%)	0.153 (3.1%)
2,4,6-octatriene	6-31G(d)	0.969 (20.0%)	0.982 (20.3%)	0.951 (19.7%)
	6-311G(d)	0.964 (20.2%)	0.992 (20.8%)	0.959 (20.2%)
pyridyl oxazole	6-31G(d)	0.467 (12.7%)	0.585 (14.8%)	0.540 (13.9%)
	6-311G(d)	0.469 (12.9%)	0.591 (15.1%)	0.545 (14.2%)
porphyrin (small)[c]	6-31G(d)	0.131 (5.7%)	0.276 (12.2%)	0.209 (9.0%)
porphyrin (large)[c]	6-31G(d)	0.267 (12.4%)	0.267 (12.4%)	0.220 (10.0%)

[a]All virtual orbitals, only those occupied orbitals that have an excitation amplitude >0.15. [b]All energies in eV. [c]Schematic structures given in the Supporting Information. [d]The truncated TDDFT calculation failed to converge to the correct state.

used within the literature. For the case of charge-transfer-like excitations, it is necessary to partition the electron repulsion operator into short-range and long-range components:

$$\frac{1}{r_{12}} = \frac{1 - \mathrm{erf}(\omega_{r_{12}})}{r_{12}} + \frac{\mathrm{erf}(\omega_{r_{12}})}{r_{12}} \quad (1)$$

where erf is the error function and $r_{12} = |\mathbf{r}_1 - \mathbf{r}_2|$. The first term on the right-hand side of eq 1 is the short-range component of the exchange and is evaluated with DFT, while the second term is the long-range component, which is evaluated with exact Hartree−Fock exchange.

All calculations were started from the ground-state minimum energy geometry as determined at the B3LYP/6-31G(d) level of theory. The TDDFT/TDA calculations were made more computationally tractable by invoking a scheme in which a truncated set of single-excitations are calculated from a selection of the molecular orbitals. In TDDFT/TDA,[34] excitation energies and oscillator strengths are calculated as solutions to the eigenvalue problem:

$$\mathbf{AX} = \omega\mathbf{X} \quad (2)$$

A subset of orbitals is chosen to yield the following equation:

$$\bar{\mathbf{A}}\mathbf{X} = \omega\mathbf{X} \quad (3)$$

where

$$\bar{\mathbf{A}} = \mathbf{A}_{\bar{a}\bar{i}\sigma,\bar{b}\bar{j}\tau} \quad (4)$$

in which $\{\bar{i}\}$ and $\{\bar{a}\}$ are subsets of the occupied and virtual orbitals, respectively.[34] The TDDFT/TDA gradients are then performed within this truncated space of orbitals. The calculations were performed within a development version of Q-Chem,[53] in which the current approach has been implemented.

In the following section, three distinct approaches are applied: in the first, all of the virtual orbitals are included in the TDDFT/TDA calculation, while only the occupied orbitals considered to be contributing in the first singlet excited state (as determined from an all-orbital TDDFT/TDA calculation with the same functional and basis set combination and all orbitals contributing and with an excitation amplitude >0.15) involved. In the second scenario, the number of virtual orbitals is reduced, while keeping the number of occupied orbitals the same as above. Finally, we allow a small increase in the number of occupied orbitals (approximately $^1/_3$ of all valence occupied orbitals), while keeping a relatively small number of virtual orbitals (~50%) within the calculation. The target for the current paper is emission energies within 0.1 eV of those produced by all-orbital TDDFT/TDA. This is a somewhat arbitrary target, and the results of this work show that significantly tighter tolerances can easily be achieved with a substantial reduction in computational effort compared to conventional TDDFT/TDA. It is worth pointing out that the current study is not intended as an investigation of the accuracy of TDDFT/TDA excited-state geometries, but rather the accuracy of cheap TDDFT/TDA geometries versus full TDDFT/TDA geometries. Further studies of the accuracy of TDDFT excited-state geometries can be found in the following refs: 54−58.

Finally, the method is applied to a derivative of an organic dye used in dye-sensitized solar cells (Carbz-PAHTDTT).[59] This structure has 151 atoms and possesses C1 symmetry (structure given in the Supporting Information). The calculation was performed with the ωB97X-D functional and 6-31G(d) basis set using both all-orbital TDDFT/TDA and reduced subspace TDDFT/TDA including all-valence occupied orbitals and the 50% lowest energy virtual orbitals.

3. RESULTS AND DISCUSSION

3.1. All virtual orbitals. Given in Table 1 are the differences in the vertical excitation energies calculated with standard TDDFT/TDA and the reduced single excitation TDDFT/TDA at the excited-state geometry calculated by the appropriate method (i.e., full TDDFT/TDA or reduced single-excitation TDDFT/TDA). Good agreement is found for the smaller molecules, formaldehyde, benzene, and naphthalene. The other molecules investigated display a poorer agreement and certainly above our arbitrary 0.1 eV threshold. One must also carefully look at the three most extreme cases. Using B3LYP to calculate the excited state geometry of indole using only the HOMO and HOMO−1 orbitals yields an incorrect electronic state, and so the result is not displayed here. The

dx.doi.org/10.1021/ct500687j | J. Chem. Theory Comput. XXXX, XXX, XXX−XXX

Table 2. Difference in the Emission Energies Calculated at the Excited State Geometry As Calculated with the Subspace TDDFT/TDA Method with the Reduced Number of Virtual Orbitals (in Italics) versus the Full TDDFT/TDA Method, Using ωB97X-D/6-311G(d)

molecule		ΔE			
formaldehyde	virtual orbs	*30/34*	*25/34*	*20/34*	*15/34*
	ΔE	0.008 (0.3%)	−0.007 (0.2%)	−0.007 (0.2%)	0.057 (1.8%)
benzene	virtual orbs	*95/105*	*80/105*	*65/105*	*50/105*
	ΔE	0.048 (0.9%)	0.049 (0.9%)	0.049 (0.9%)	0.061 (1.1%)
naphthalene	virtual orbs	*150/170*	*130/170*	*105/170*	*85/170*
	ΔE	0.106 (2.3%)	0.106 (2.3%)	0.105 (2.3%)	0.111 (2.5%)
2,4,6-octatriene	virtual orbs	*130/150*	*115/150*	*95/150*	*75/150*
	ΔE	0.959 (20.2%)	0.961 (20.2%)	0.959 (20.2%)	0.958 (20.2%)
pyridyl oxazole	virtual orbs	*245/281*	*210/281*	*175/281*	*140/281*
	ΔE	0.545 (14.2%)	0.546 (14.2%)	0.547 (14.2%)	0.547 (14.2%)
porphyrin (small)[a]	virtual orbs	*270/307*	*230/307*	*190/307*	*150/307*
	ΔE	0.209 (9.0%)	0.210 (9.0%)	0.210 (9.0%)	0.211(9.1%)

[a]The 6-31G(d) basis was used.

Table 3. Emission Energy Differences Calculated between Conventional TDDFT/TDA and the Reduced Subspace TDDFT/TDA ($^1/_3$ of All Valence Orbitals, 50% of All Virtual Orbitals) at the First Singlet Excited-State Geometry Calculated with the Respective Method[a]

		functional		
molecule	basis set	B3LYP	LRC-ωPBE	ωB97X-D
formaldehyde	6-31G(d)	0.014 (0.5%)	0.020 (0.7%)	0.007 (0.2%)
	6-311G(d)	0.005 (0.2%)	0.019 (0.6%)	−0.008 (0.3%)
benzene	6-31G(d)	0.041 (0.8%)	0.049 (0.9%)	0.046 (0.8%)
	6-311G(d)	0.045 (0.9%)	0.056 (1.0%)	0.053 (1.0%)
naphthalene	6-31G(d)	0.025 (0.6%)	0.044 (1.0%)	0.030 (0.7%)
	6-311G(d)	0.029 (0.7%)	0.051 (1.1%)	0.036 (0.8%)
indole	6-31G(d)	[c]	0.112 (2.2%)	0.107 (2.1%)
	6-311G(d)	[c]	0.120 (2.4%)	0.115 (2.3%)
2,4,6-octatriene	6-31G(d)	0.424 (8.7%)	0.485 (10.0%)	0.476 (9.9%)
	6-311G(d)	0.436 (9.1%)	0.505 (10.6%)	0.493 (10.4%)
pyridyl oxazole	6-31G(d)	0.221 (6.0%)	0.276 (7.0%)	0.264 (6.8%)
	6-311G(d)	0.219 (6.0%)	0.278 (7.1%)	0.264 (6.9%)
porphyrin (small)[ba]	6-31G(d)	0.041 (1.8%)	0.068 (3.0%)	0.054 (2.3%)
porphyrin (large)[ba]	6-31G(d)	0.019 (0.9%)	0.057 (2.6%)	0.041 (1.4%)

[a]All energies in eV. [ba]Schematic structures given in the Supporting Information. [c]The truncated TDDFT calculation failed to converge to the correct state.

description of the correct emitting state of indole using TD-B3LYP is well-known to be troublesome with all orbitals included, and so, the result obtained here comes as no surprise.[40,60−62] Indeed, the ^1L_a and ^1L_b states are calculated to be very close even with the highly accurate CASPT2 approach.[63] Each of the functionals performs equally poorly for 2,4,6-octatriene and pyridyl oxazole, with the maximum error here being nearly 1 eV. If one considers first 2,4,6-octatriene, then it is clear that a significant number of occupied orbitals participate in the full TDDFT/TDA description of the first singlet excited-state (see Supporting Information). The dominant HOMO → LUMO transition (94.9%) is captured using the minimum occupied orbital approach outlined here, but significant contributions from other orbitals are behind the very large error versus the all-orbital TDDFT approach. One finds a similar explanation behind the large error for pyridyl oxazole.

3.2. Reduced Space of Virtual Orbitals. Presented in Table 2 are the vertical excitation energies calculated at the excited state geometry, which was obtained using the subspace TDDFT/TDA with a reduced number of virtual orbitals for ωB97X-D; the other functionals displayed similar results (data not shown). The result here is encouraging; even with only 50% of the virtual orbitals included, none of the errors increases by more than 0.02 eV, except for formaldehyde (∼0.06 eV increase). This data points to the importance of including the occupied orbitals more so than the full virtual space, as evidenced by the case of 2,4,6-ocatriene above.

3.3. Increased Number of Occupied Orbitals. From Table 1 it is evident that, as the size of the molecule becomes larger, using just one or two occupied orbitals within the TDDFT/TDA calculation becomes significantly less accurate. Certainly, Table 2 backs this up, with little or no change in accuracy of the emission energy when the number of virtual orbitals included is halved. Following the same protocol as previously, we increase the number of occupied orbitals included within the TDDFT/TDA calculation, while keeping the number of virtual orbitals included at about 50% of the total number of virtual orbitals. These data are presented in Table 3. It can be seen that most of the errors in comparison to all-orbital TDDFT/TDA are less than 0.1 eV, except for indole, 2,4,6-octatriene and pyridyl oxazole. If we once again consider

dx.doi.org/10.1021/ct500687j | J. Chem. Theory Comput. XXXX, XXX, XXX−XXX

Table 4. Emission Energy Differences Calculated between Conventional TDDFT/TDA and the Reduced TDDFT/TDA ($^1/_3$ of All Valence Orbitals, 50% of All Virtual Orbitals) at the First Singlet Excited-State Geometry Calculated with the Respective Method[a]

		functional		
molecule	basis set	B3LYP	LRC-ωPBE	ωB97X-D
indole	6-31G(d)	0.004 (0.1%)	0.009 (0.2%)	0.009 (0.2%)
	6-311G(d)	0.005 (0.1%)	0.016 (0.3%)	0.014 (0.3%)
2,4,6-octatriene	6-31G(d)	0.020 (0.4%)	0.028 (0.6%)	0.028 (0.6%)
	6-311G(d)	0.035 (0.7%)	0.058 (1.2%)	0.050 (1.0%)
pyridyl oxazole	6-31G(d)	0.005 (0.1%)	0.007 (0.2%)	0.007 (0.2%)
	6-311G(d)	0.008 (0.2%)	0.014 (0.3%)	0.013 (0.3%)

[a]All energies in eV.

Table 5. Average and Maximum Errors in Bond Lengths and Angles of the Molecules Considered with the Minimum Number of Orbitals Included within the TDDFT/TDA Subspace and with an Increased Number of Orbitals within the Subspace[a]

	min. no. of orbitals				increased no. of orbitals			
	bond length (Å)		angle (deg)		bond length (Å)		angle (deg)	
molecule	$\bar{\varepsilon}$	ε_{max}	$\bar{\varepsilon}$	ε_{max}	$\bar{\varepsilon}$	ε_{max}	$\bar{\varepsilon}$	ε_{max}
formaldehyde	0.008	0.010	1.46	2.64	0.008	0.010	1.49	2.77
benzene	0.000	0.000	0.00	0.00	0.000	0.000	0.01	0.02
naphthalene	0.001	0.002	0.07	0.12	0.000	0.000	0.01	0.02
indole	0.002	0.006	0.20	0.47	0.000	0.001	0.01	0.05
2,4,6-octatriene	0.003	0.019	0.24	0.73	0.000	0.001	0.07	0.15
pyridyl oxazole	0.002	0.010	0.11	0.42	0.000	0.000	0.01	0.03
porphyrin (small)	0.001	0.002	0.05	0.19	0.000	0.000	0.05	0.47
porphyrin (large)	0.001	0.003	0.04	0.25	0.003	0.006	0.11	0.30

[a]See main text for details.

2,4,6-octatriene, the error has been halved with respect to the data in Table 1, although it is still unacceptably high. The same is also true for pyridyl oxazole.

Table 4 shows the errors in the emission energies when all valence occupied orbitals and 50% of the virtual orbitals are included. There is a huge improvement for each molecule/method combination, with a maximum error of just 0.058 eV for 2,4,6-octatriene (LRC-ωPBE/6-311G(d)). The mean deviations from all-orbital TDDFT/TDA are less than 0.01 eV for both indole and pyridyl oxazole, and less than 0.04 eV for 2,4,6-octatriene.

3.4. General Discussion. The data presented above has focused on the errors in the calculated emission energies as an indicator of the accuracy of the excited state geometries. Mean and maximum deviations of the geometrical parameters for each of the scenarios above are presented in the Supporting Information, with the data for ωB97X-D/6-31G(d) given in Table 5. Figure 1 displays the relationship between the RMSD error of the internal coordinates with the error in the emission energy. While there is no simple analytical relationship, there is a qualitative relationship between the emission energy and the accuracy of the obtained geometry. This is borne out by close inspection of the data in the Supporting Information. Where there are large errors in the calculated emission energy (e.g., 2,4,6-octatriene), there are also large errors in the geometrical parameters (see Supporting Information Tables S1 and S2). On inclusion of more occupied orbitals, the deviation found in the geometrical parameters reduces significantly (Supporting Information Tables S3 and S4). To understand whether these effects were due to geometrical concerns or the quality of the reduced subspace TDDFT/TDA energies, additional calculations were performed in which the reduced subspace

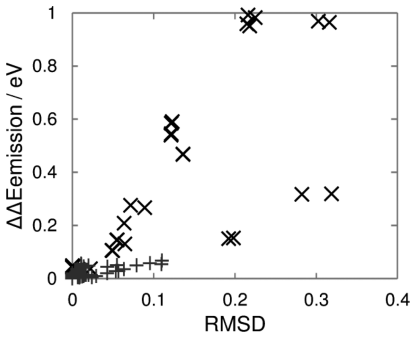

Figure 1. RMSD of the internal coordinates (z-matrix) versus the difference in emission energy calculated with full TDDFT/TDA and truncated TDDFT/TDA.

TDDFT/TDA emission energies were calculated at the geometries obtained with the all-orbital TDDFT/TDA approach, and vice versa. The average error was 0.029 eV with a maximum error of 0.054 eV. Thus, we can conclude that a poor starting reduced subspace TDDFT/TDA energy leads to a very different geometry to that calculated with the all-orbital approach. While computational time and resources are already known to be reduced within the TDDFT/TDA energy module,[34] there is also a substantial saving in CPU time of between 15 and 30% while calculating the reduced orbital space TDDFT/TDA gradients.

The calculation with the derivative of the Carbz-PAHTDTT dye-sensitizer molecule (Figure 2) demonstrated the efficacy of the current proposal—the emission energy was underestimated by just 0.016 eV (1.1%) with average and maximum errors in the bond lengths and bond angles of 0.001 Å, 0.003 Å, 0.11° and 0.40°, respectively. The saving in CPU time was ∼28%,

dx.doi.org/10.1021/ct500687j | J. Chem. Theory Comput. XXXX, XXX, XXX−XXX

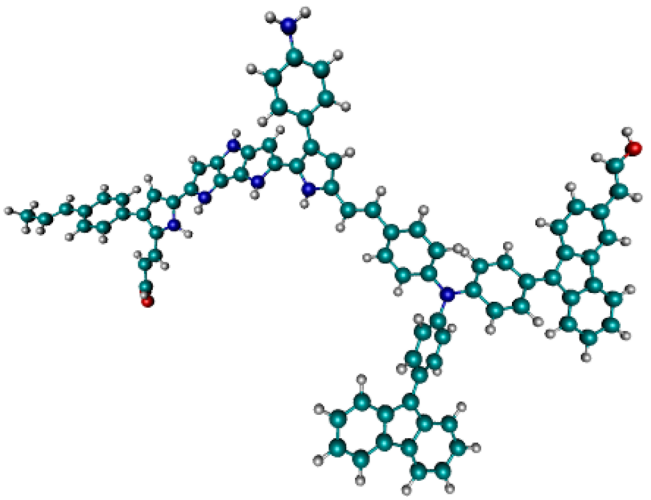

Figure 2. Molecular structure of the Carbz-PAHTDTT derivative.

which is reasonable given that all valence occupied orbitals were included.

The optimal strategy for employing this scheme would be to test which orbitals are involved in the state(s) of interest using only the valence occupied and half of the virtual orbitals in a single-point vertical excitation energy calculation. Tests can then be performed with reduced numbers of occupied orbitals (see Figures 1 and 3) until the desired balance of accuracy

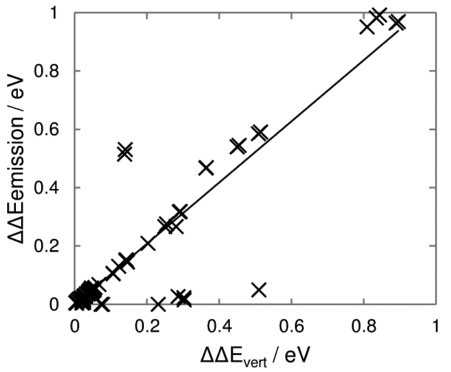

Figure 3. Difference in vertical excitation energy between full TDDFT/TDA and the truncated TDDFT/TDA versus the difference in the emission energy between full TDDFT/TDA and truncated TDDFT/TDA.

versus computational resource can be established. This scheme is implemented within the development version of Q-Chem we are currently using.

4. CONCLUSIONS

The work presented here shows the efficacy of employing the reduced subspace TDDFT/TDA method to the calculation of excited state geometries. Substantial savings in computational resources have been made, while the maximum deviation from all-orbital TDDFT/TDA of less than 0.04 eV in the emission energy, less than 0.01 Å in bond-lengths and less than 0.5° in bond angles is found across all molecules considered here (except formaldehyde, which has a maximum deviation of 2° in the bond angle from all-orbital TDDFT/TDA). Encouragingly, this success is repeated on the largest molecule considered here, for which the maximum efficiency gains were found. The same general trends have been found independent of the choice of functional and basis set, except for the case of indole, in which B3LYP is known to fail.

■ ASSOCIATED CONTENT

Supporting Information

Deviations from full TDDFT/TDA geometrical parameters, orbital plots and Cartesian coordinates for the Carbz-PAHTDTT derivative are available. This material is available free of charge via the Internet at http://pubs.acs.org.

■ AUTHOR INFORMATION

Corresponding Author

*E-mail: david.robinson@nottingham.ac.uk.

Notes

The authors declare no competing financial interest.

■ ACKNOWLEDGMENTS

I am grateful to the University Of Nottingham for provision of time on the Minerva High Performance Computing cluster.

■ REFERENCES

(1) See, for example, Roos, B. O. The complete active space self-consistent field method and its applications in electronic structure calculations. *Adv. Chem. Phys.* **1987**, *69*, 399−442.

(2) Andersson, K.; Malmqvist, P.-Å.; Roos, B. O.; Sadlej, A. J.; Wolinski, K. Second-order perturbation theory with a CASSCF reference function. *J. Phys. Chem.* **1990**, *94*, 5483−5488.

(3) Andersson, K.; Malmqvist, P.-Å.; Roos, B. O. Second-order perturbation theory with a complete active space self-consistent field reference function. *J. Chem. Phys.* **1992**, *96*, 1218−1226.

(4) Hirao, K. Multireference Møller—Plesset method. *Chem. Phys. Lett.* **1992**, *190*, 374−380.

(5) Hirao, K. Multireference Møller—Plesset perturbation theory for high-spin open-shell systems. *Chem. Phys. Lett.* **1992**, *196*, 397−403.

(6) Angeli, C.; Cimiraglia, R.; Evangelisti, S.; Leininger, T.; Malrieu, J. P. Introduction of n−electron valence states for multireference perturbation theory. *J. Chem. Phys.* **2001**, *114*, 10252−10264.

(7) Angeli, C.; Cimiraglia, R.; Malrieu, J. P. n−Electron valence state perturbation theory: A fast implementation of the strongly contracted variant. *Chem. Phys. Lett.* **2001**, *350*, 297−305.

(8) Angeli, C.; Cimiraglia, R.; Malrieu, J. P. n−Electron valence state perturbation theory: A spinless formulation and an efficient implementation of the strongly contracted and of the partially contracted variants. *J. Chem. Phys.* **2002**, *117*, 9138−9153.

(9) Aquilante, F.; Malmqvist, P. −Å.; Pederson, T. B.; Ghosh, A.; Roos, B. O. Cholesky decomposition-based multiconfiguration second-order perturbation theory (CD-CASPT2): Application to the spin-state energetics of CoIII(diiminato)(NPh). *J. Chem. Theory Comput.* **2008**, *4*, 694−702.

(10) Malmqvist, P. −Å.; Pierloot, K.; Shahi, A. R. M.; Cramer, C. J.; Gagliardi, L. The restricted active space followed by second-order perturbation theory method: Theory and application to the study of CuO_2 and Cu_2O_2 systems. *J. Chem. Phys.* **2008**, *128*, 204109.

(11) Sauri, V.; Serrano-Andrés; Shahi, A. R. M.; Gagliardi, L.; Vancoillie, S.; Pierloot, K. Multiconfigurational second-order perturbation theory restricted active space (RASPT2) method for electronic excited states: A benchmark study. *J. Chem. Theory Comput.* **2011**, *7*, 153−168.

(12) Robinson, D.; McDouall, J. J. W. Multireference perturbation theory applied to multiconfigurational problems: Is the CASSCF step necessary? *Mol. Phys.* **2006**, *104*, 681−690.

(13) Robinson, D.; McDouall, J. J. W. CASCI reference wave functions for multireference perturbation theory built from Hartree−Fock or Kohn−Sham orbitals. *J. Chem. Theory Comput.* **2007**, *3*, 1306−1311.

(14) Robinson, D.; McDouall, J. J. W. Simplified reference wave functions for multireference perturbation theory. *J. Phys. Chem. A* **2007**, *111*, 9815−9822.
(15) Stanton, J. F.; Bartlett, R. J. The equation of motion coupled-cluster method. A systematic biorthogonal approach to molecular excitation energies, transition probabilities, and excited state properties. *J. Chem. Phys.* **1993**, *98*, 7029−7039.
(16) Krylov, A. I.; Sherrill, C. D.; Head-Gordon, M. Excited states theory for optimized orbitals and valence optimized orbitals coupled-cluster doubles models. *J. Chem. Phys.* **2000**, *113*, 6509−6527.
(17) Koch, H.; Jensen, H. J. A.; Jørgensen, P.; Helgaker, T. Excitation energies from the coupled cluster singles and doubles linear response function (CCSDLR). Applications to Be, CH^+, CO, and H_2O. *J. Chem. Phys.* **1990**, *93*, 3345−3350.
(18) Levchenko, S. V.; Krylov, A. I. Equation-of-motion spin-flip coupled-cluster model with single and double substitutions: Theory and application to cyclobutadiene. *J. Chem. Phys.* **2004**, *120*, 175−185.
(19) Krylov, A. I. Size-consistent wave functions for bond-breaking: The equation-of-motion spin-flip model. *Chem. Phys. Lett.* **2001**, *338*, 375−384.
(20) Sinha, D.; Mukhopadhya, D.; Chaudhuri, R.; Mukherjee, D. The eigenvalue-independent partitioning technique in Fock space: An alternative route to open-shell coupled-cluster theory for incomplete model spaces. *Chem. Phys. Lett.* **1989**, *154*, 544−549.
(21) Stanton, J. F.; Gauss, J. Analytic energy derivatives for ionized states described by the equation-of-motion coupled cluster method. *J. Chem. Phys.* **1994**, *101*, 8938−8944.
(22) Nooijen, M.; Bartlett, R. J. Equation of motion coupled cluster method for electron attachment. *J. Chem. Phys.* **1995**, *102*, 3629−3647.
(23) Rappoport, D.; Furche, F. Photoinduced intramolecular charge transfer in 4-(dimethyl)aminobenzonitrile - A theoretical perspective. *J. Am. Chem. Soc.* **2004**, *126*, 1277−1284.
(24) Guido, C. A.; Mennucci, B.; Jacquemin, D.; Adamo, C. Planar vs twisted intramolecular charge transfer mechanism in Nile Red: New hints from theory. *Phys. Chem. Chem. Phys.* **2010**, *12*, 8016−8023.
(25) Blake, H.; Robinson, D. QM/MM Studies of Contemporary and Novel Membrane Raft Fluorescent Probes. *Molecules* **2014**, *19*, 10230−10241.
(26) Jamorski, C. J.; Casida, M. E. Time-dependent density-functional theory investigation of the fluorescence behavior as a function of alkyl chain size for the 4-(N,N-dimethylamino)-benzonitrile-like donor−acceptor systems 4-(N,N-diethylamino)-benzonitrile and 4-(N,N-diisopropylamino)benzonitrile. *J. Phys. Chem. B* **2004**, *108*, 7132−7141.
(27) Sheng, Y.; Leszczynski, J. Comprehensive theoretical study of the conversion reactions of spiropyrans: Substituent and solvent effects. *J. Phys. Chem. B* **2004**, *108*, 16233−16243.
(28) Jacquemin, D.; Planchat, A.; Adamo, C.; Mennucci, B. TD-DFT assessment of functionals for optical 0−0 transitions in solvated dyes. *J. Chem. Theory Comput.* **2012**, *8*, 2359−2372.
(29) Van Caillie, C.; Amos, R. D. Geometric derivatives of density functional theory excitation energies using gradient-corrected functionals. *Chem. Phys. Lett.* **2000**, *317*, 159−164.
(30) Dreuw, A.; Head-Gordon, M. Failure of time-dependent density functional theory for long-range charge-transfer excited states: The zincbacteriochlorin−bacteriochlorin and bacteriochlorophyll−spheroidene complexes. *J. Am. Chem. Soc.* **2004**, *126*, 4007−4016.
(31) Gilbert, A. T. B.; Besley, N. A.; Gill, P. M. W. Self-consistent field calculations of excited states using the maximum overlap method (MOM). *J. Phys. Chem. A* **2008**, *112*, 13164−13172.
(32) Hirata, S.; Head-Gordon, M. Time-dependent density functional theory within the Tamm−Dancoff approximation. *Chem. Phys. Lett.* **1999**, *314*, 291−299.
(33) Moore, B., II; Autschbach, J. Longest-wavelength electronic excitations of linear cyanines: The role of electron delocalization and of approximations in time-dependent density functional theory. *J. Chem. Theory Comput.* **2013**, *9*, 4991−5003.
(34) Besley, N. A. Calculation of the electronic spectra of molecules in solution and on surfaces. *Chem. Phys. Lett.* **2004**, *390*, 124−129.
(35) Besley, N. A.; Oakley, M. T.; Cowan, A. J.; Hirst, J. D. A sequential molecular mechanics/quantum mechanics study of the electronic spectra of amides. *J. Am. Chem. Soc.* **2004**, *126*, 13502−13511.
(36) Robinson, D.; Besley, N. A.; O'Shea, P.; Hirst, J. D. Electronic structure of 5-hydroxyindole: From gas phase to explicit solvation. *J. Phys. Chem. B* **2009**, *113*, 2535−2541.
(37) Besley, N. A. Theoretical study of the electronic spectroscopy of CO adsorbed on Pt(111). *J. Chem. Phys.* **2005**, *122*, 184706.
(38) Besley, N. A.; Blundy, A. J. Electronic excited states of Si(100) and organic molecules adsorbed on Si(100). *J. Phys. Chem. B* **2006**, *110*, 1701−1710.
(39) Besley, N. A.; Noble, A. Time-dependent density functional theory study of the X-ray absorption spectroscopy of acetylene, ethylene, and benzene on Si(100). *J. Phys. Chem. C* **2007**, *111*, 3333−3340.
(40) Rogers, D. M.; Besley, N. A.; O'Shea, P.; Hirst, J. D. Modeling the absorption spectrum of tryptophan in proteins. *J. Phys. Chem. B* **2005**, *109*, 23061−23069.
(41) Robinson, D.; Besley, N. A.; O'Shea, P.; Hirst, J. D. Calculating the fluorescence of 5-hydroxytryptophan in proteins. *J. Phys. Chem. B* **2009**, *113*, 14521−14528.
(42) Robinson, D.; Besley, N. A. Modelling the spectroscopy and dynamics of plastocyanin. *Phys. Chem. Chem. Phys.* **2010**, *12*, 9667−9676.
(43) Besley, N. A.; Robinson, D. Theoretical simulation of the spectroscopy and dynamics of a red copper protein. *Faraday Discuss.* **2011**, *148*, 55−70.
(44) Robinson, D.; Besley, N. A.; O'Shea, P.; Hirst, J. D. Di-8-ANEPPS Emission Spectra in Phospholipid/Cholesterol Membranes: A Theoretical Study. *J. Phys. Chem. B* **2011**, *115*, 4160−4167.
(45) Asmuruf, F. A.; Besley, N. A. Time dependent density functional theory study of the near-edge X-ray absorption fine structure of benzene in gas phase and on metal surfaces. *J. Chem. Phys.* **2008**, *129*, 064705.
(46) Asmuruf, F. A.; Besley, N. A. Density functional theory study of the near edge X-ray absorption fine structure and infrared spectroscopy of acetylene and benzene on group IV semiconductor surfaces. *Surf. Sci.* **2009**, *603*, 158−164.
(47) Besley, N. A.; Peach, M. J. G.; Tozer, D. J. Time-dependent density functional theory calculations of near-edge X-ray absorption fine structure with short-range corrected functionals. *Phys. Chem. Chem. Phys.* **2009**, *11*, 10350−10358.
(48) Becke, A. D. Density-functional thermochemistry. III. The role of exact exchange. *J. Chem. Phys.* **1993**, *98*, 5648−5652.
(49) Henderson, T. M.; Janesko, B. G.; Scuseria, G. E. Generalized gradient approximation model exchange holes for range-separated hybrids. *J. Chem. Phys.* **2008**, *128*, 194105.
(50) Chai, J.-D.; Head-Gordon, M. Long-range corrected hybrid density functionals with damped atom−atom dispersion corrections. *Phys. Chem. Chem. Phys.* **2008**, *10*, 6615−6620.
(51) Hariharan, P. C.; Pople, J. A. Influence of polarization functions on molecular-orbital hydrogenation energies. *Theoret. Chim. Acta* **1973**, *28*, 213−222.
(52) Krishnan, R.; Binkley, J. S.; Seeger, R.; Pople, J. A. Self-consistent molecular orbital methods. XX. A basis set for correlated wave functions. *J. Chem. Phys.* **1980**, *72*, 650−654.
(53) Krylov, A. I.; Gill, P. M. W. Q-Chem: An engine for innovation. *WIREs Comput. Mol. Sci.* **2013**, *3*, 317−326.
(54) Furche, F.; Ahlrichs, R. Adiabatic time-dependent density functional methods for excited state properties. *J. Chem. Phys.* **2002**, *117*, 7433−7447.
(55) Aquino, A. J. A.; Lischka, H. Excited-state intramolecular proton transfer: A survey of TDDFT and RI-CC2 excited-state potential energy surfaces. *J. Phys. Chem. A* **2005**, *109*, 3201−3208.
(56) Liu, F.; Gan, Z.; Shao, Y.; Hsu, C.-P.; Dreuw, A.; Head-Gordon, M.; Miller, B. T.; Brooks, B. R.; Yu, J.-G.; Furlani, T. R.; Kong, J. A parallel implementation of the analytic nuclear gradient for time-

dependent density functional theory within the Tamm−Dancoff approximation. *Mol. Phys.* **2010**, *108*, 2791−2800.
(57) Bousquet, D.; Fukuda, R.; Maitarad, P.; Jacquemin, D.; Ciofini, I.; Adamo, C.; Ehara, M. Excited-state geometries of heteroaromatic compounds: Comparative TDDFT and SAC-CI study. *J. Chem. Theory Comput.* **2013**, *9*, 2368−2379.
(58) Guido, C. A.; Knecht, S.; Kongsted, J.; Menucci, B. Benchmarking TDDFT for excited-state geometries of organic molecules in gas-phase and in solution. *J. Chem. Theory Comput.* **2013**, *9*, 2209−2220.
(59) Daeneke, T.; Kwon, T.-H.; Holmes, A. B.; Duffy, N. W.; Bach, U.; Spiccia, L. High-efficiency dye-sensitized solar cells with ferrocene-based electrolytes. *Nat. Chem.* **2011**, *3*, 211−215.
(60) Arulmozhiraja, S.; Coote, M. L. ^1L_a and ^1L_b states of indole and azaindole: Is density functional theory inadequate? *J. Chem. Theory Comput.* **2012**, *8*, 575−584.
(61) Wiggins, P.; Williams, J. A. G.; Tozer, D. J. Excited state surfaces in density functional theory: A new twist on an old problem. *J. Chem. Phys.* **2009**, *131*, 091101.
(62) Plötner, J.; Tozer, D. J.; Dreuw, A. Dependence of excited state potential energy surfaces on the spatial overlap of the Kohn−Sham orbitals and the amount of nonlocal Hartree−Fock exchange in time-dependent density Functional Theory. *J. Chem. Theory Comput.* **2010**, *6*, 2315−2324.
(63) Serrano-Andrés, L.; Roos, B. O. Theoretical study of the absorption and emission spectra of indole in the gas phase and in a solvent. *J. Am. Chem. Soc.* **1996**, *118*, 185−195.